International Journal of Environmental Sciences
ISSN: 2229-7359
Vol. 11 No. 9s, 2025
https://theaspd.com/index.php

Application Of Densenet Architecture And Its Variants Towards Breast Cancer Detection: A Multi-View Analysis

Pratibha T Joshi [a]; * Gurpreet Singh Saini [b]; Shivaji D Pawar[a], Research Scholar, Lovely Professional University,
[a]Punjab, and Department of Electronics and Telecomm SIES GST, Nerul, Navi Mumbai, India, Pratibhaj@sies.edu.in
[b] School of Electronics and Electrical Engineering, Lovely Professional University, Punjab,gurpreet.16889@lpu.co.inc
[c] School of AI and Future Technologies, Universal AI University Karjat, Mumbai, India,shivaji.pawar@universalai.in

Abstract
Artificial Intelligence has made giant strides in medical image classification using the development of Convolutional Neural Networks (CNNs) in the past decade. Different CNN architectures like Dense-Net Res-Net, etc., are used in the medical industry to identify patterns and features leading to a faster diagnosis. The fundamental motivation behind this research article is to study the application of different variants of Dense-Net architecture (DenseNet121, 169, and 201) towards breast cancer detection and provide a comparative analysis of Dense-net variants to the intended area of research with the support of digital mammography two mediolateral oblique (MLO). Two craniocaudal (CC) views of a single patient are used to extract the distinct features of breast cancer detection. The proposed research utilizes 9695 digital mammography images for this study. All input images are classified into three categories, Benign, Cancer, and Normal, with the help of expert radiologists as ground truth. All the proposed classifier's performances are tested with different testing matrices such as precision, responsiveness, and specificity. The concluding results demonstrate that these intended Dense-net architecture variants have delivered an exemplary performance with the highest accuracy of 94.90 % during training and 96.924% during testing on CC views. Precision, Recall, and F1 scores are 0.965, 0.969, and 0.967, respectively. A comparative analysis of the proposed model with its variants and other state-of-the-art methods is provided. Comparative research shows that DenseNet architecture can provide more accurate results when only left CC views are used as input. Acquired outcomes are again validated qualitatively with a radiologist expert in the field of breast cancer. The proposed architecture achieved state-of-the-art results with a fewer number of images and with less computation
Keywords: *Breast cancer, Classification accuracy, Digital mammography, Dense-Net architecture, deep learning.*

INTRODUCTION

Breast cancer is the world's fifth highest standard casualty rate (685,000) among all diseases. In the last five years, 7.8 million women were healed of breast cancer and survived. Breast cancer can occur in women of any generation [1-2]. Nevertheless, it is more expected in older eras. Early diagnosis is crucial in breast cancer, as with all cancer types. Early diagnosis of breast cancer contributes to a reduction in the frequency of premature deaths [3]. Different image detection modalities such as Digital Mammography, Magnetic resonance imaging (MRI), Molecular breast imaging (MBI), and Breast biopsy are used to detect and predict breast cancer with the support of expert radiologists [4]. Figure 1 depicts the different breast cancer classifications.

International Journal of Environmental Sciences
ISSN: 2229-7359
Vol. 11 No. 9s, 2025
https://theaspd.com/index.php

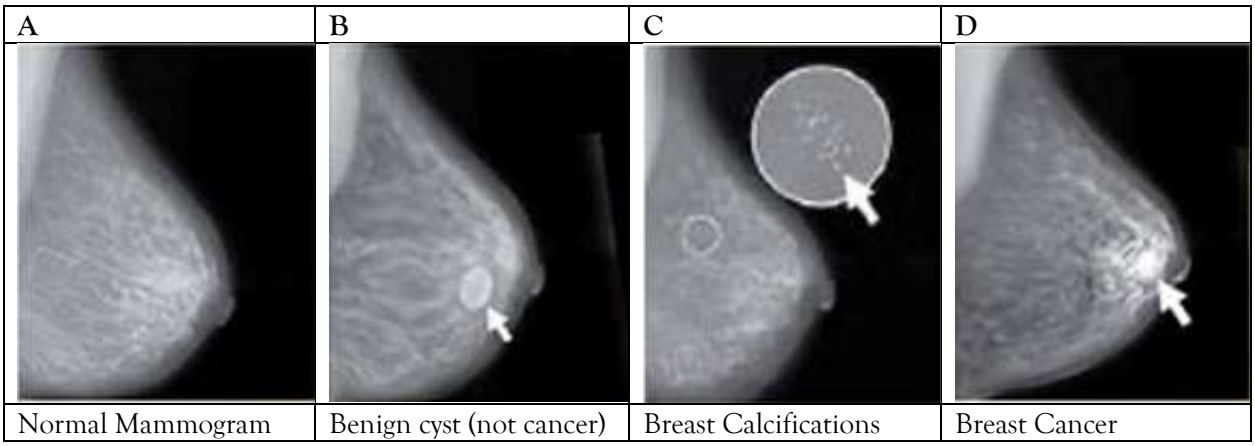

Fig.1 - Breast cancer classification (Image Courtesy National cancer institute)

Four views of the input raw digital mammography are shown in figure-2. All the views have equal significance in breast cancer detection. A single patient's two mediolateral oblique (MLO) and two craniocaudal (CC) views are used to extract the distinct features of breast cancer detection [5].

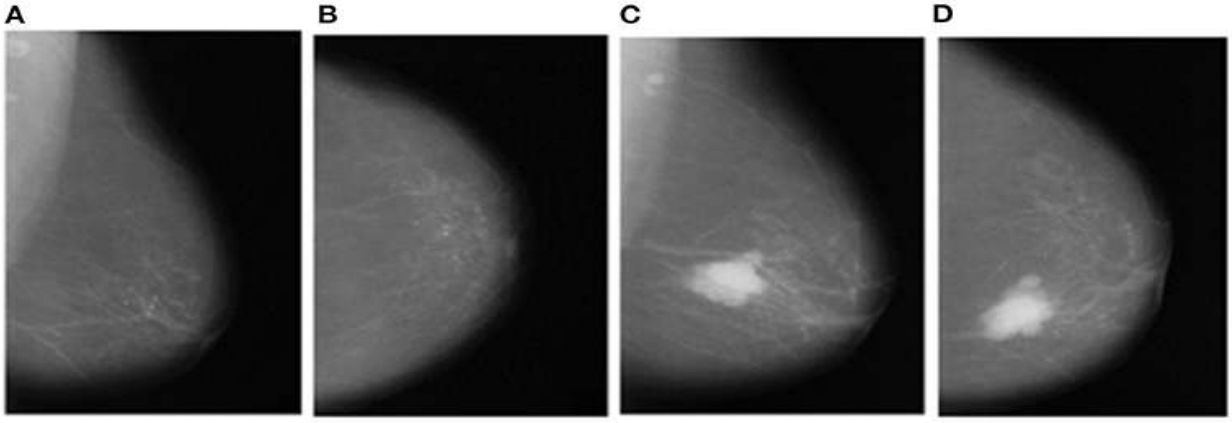

Fig.2- Input raw images- (A) Left_MLO (B) Left_CC (C) Right_MLO (D) Right_CC.

Many study research efforts have been in advancement for an automatic objective inspection of breast cancer over the previous few decades. The preliminary stage investigation concentrates on image analysing methods such as area-based thresholding, region growing, and clustering algorithms. [6,7] Machine learning (ML) techniques based on different retrieved image topographies from the histogram, texture intensities, patterns, and image acquisition characteristics appeared as a significant work. Deep learning (DL) algorithms provide another advancement in identifying breast cancer. The fundamental merits of deep learning algorithms are that they can go substantially more in-depth and find all the meaningful attributes inside the image. Due to increased system architecture and hardware capacity, it is effortless to train DL algorithms more intensely to act as a more efficient tool for breast image analysis. With this enhancement, DL architecture becomes an excellent tool for analyzing medical images. Numerous DL techniques, such as Google-Net, Res-Net, VGG19, Residual networks, and Dense-Net, are recorded in the literature [8]. However, the "vanishing gradient problem" is a curse for deep learning algorithms as the network goes profound. Dense-Net architecture has

recently provided a novel solution to the connectivity problem. The interface of Dense-Net unites all the layers, determining on distinct map dimensions in feed-forward type; [9] hence, the distinct layer receives input from all the previous layers and conveys its map to all the farther layers. Therefore, the Dense Net join feature map passes via all the following layers instead of outlining attributes such as ResNet. This concept includes L (L+1)/2 connections instead of L, recognizing a dense connectivity pattern [10]. The result of this connectivity principle, i.e., Dense Net architecture, delivers the subsequent benefits:

1. Adequate resolution for gradient vanishing.
2. Merger in characteristic distribution.
3. Facility of feature recycling.
4. There is a meaningful decrease in training parameters.
5. Leisurely to train and produces comparable parameter efficiency.

Due to these edges, employing this model without pretraining for medical image analysis is helpful. The essential target of this research study is to analyze various variants of the dense net architecture for breast cancer detection and compare inter-variant performance with other existing methods. The research article flow hereafter follows: Section 2 describes the related work; Section 3 depicts the dataset; Section 4 shows the proposed methodology; and Section 5& 6 highlights the results and discussion. Finally, Section 7 concludes the research article with a conclusion and future scope.

Related Work

Over the last decade, breast cancer detection and deep learning have become integral to the research domain. This section discusses various previous deep learning approaches to understand the background of the intended area of research. The principal intention is to enhance the classification of deep learning classifiers. Another novel approach was recommended by Eroğlu et al. [11]. In a CNN-based categorization system, the study's main goal was to diagnose breast cancer using digital mammography, divided into three categories (benign, malignant, and normal). The proposed system used three CNN models, the Alexnet, MobilenetV2, and Resnet50, which acted as the Hybrid structure's foundation. The most valuable characteristics were then selected using the mRMR (Minimum Redundancy Maximum Relevance) feature selection approach and categorized using ML classifiers like SVM and KNN. Their investigation used 780 digital mammography images, and the SVM classifier achieved the highest accuracy: 95.60%. Shen et al. [12] suggested a CNN Model to detect cancer status on the DDSM and INbreast datasets. The proposed model has an AUC of 0.91, a sensitivity of 86.1%, and a specificity of 80.1% on the DDSM dataset. The same model has an AUC of 0.98, a sensitivity of 86.1%, and a specificity of 96.1%. Ragab et al. [13] projected a new AlexNet, a deep convolutional neural network (DCNN) type architecture. This network was fine-tuned to only two classes rather than 1000, and to gain better accuracy, the last fully connected layer was then connected to the support vector machine (SVM). The two databases used were Digital Database for Screening Mammography (DDSM); and the Curated Breast Imaging Subset of DDSM (CBIS-DDSM). When manually cropping the ROI from the mammography, the accuracy of the newly trained DCNN architecture was 71.01 percent. The samples acquired using two segmentation algorithms, cropping and rotation, had the most significant area under the curve (AUC) of 0.88 (88%). Moreover, the accuracy of the DCNN was raised to 73.6 percent when images from the CBIS-DDSM were used. As a result, the SVM accuracy increased to 87.2 percent, with an AUC of 0.94. (94 per cent).A three-stage deep learning methodology for mammography evaluation was developed by Dhungel et al. [14] In the proposed approach, mass detection was carried out by various deep learning techniques, which were improved through Bayesian optimization. Second, a level set technique intended for mass segmentation improved a deep structured output learning. The final step involved mass classification, which was accomplished using a DL classifier that had been pre-trained using regression and was then adjusted based on the labels of the breast mass classification dataset. The proposed model was tested on the

INbreast dataset, and the results were as follows. According to the system's results, 90 percent of masses could be found with one false positive per image, a segmentation accuracy of 80 to 85 percent, and final classification (as benign or malignant) that reaches a sensitivity (Se) of 0.98 and a specificity (Sp) of 0.7. AUC - 0.76.Zheng et al. [15] suggested a three-step recurrent neural network (RNN)-based CAD system to improve breast cancer identification. The first step included localizing the potentially malignant areas. The three detecting algorithms that were used were the Haar features and Viola-Jones Algorithm, Local Binary Pattern and Histograms of Oriented Grading. Secondly, the regional photos of these suspicious areas would be input into a pre-trained CNN model (pre-trained on the ImageNet dataset) for feature extraction. For this study, four different CNNs were used to compare them. They were VGG-19, ResNet50, DenseNet201 and Inception ResNetV2. Three separate scans—a registered scan, a current scan, and the difference between the two scans as the third image—were used to extract these features. Finally, an RNN classifier that can consider numerous follow-up scans and serve as a temporal assessment is trained using these three images. Although the proposed method used ResNet50 as the CNN to be used, DenseNet201 narrowly surpassed the working of all other CNNs, giving an accuracy of 0.993 compared to ResNet50's 0.991. The reason ResNet50 is proposed is that ResNet50 takes the least time for feature extraction and does it in nearly one-third the time that DenseNet201 takes. The novel idea used in this system is that it uses the current and a past scan of a subject for better and more efficient learning, which helps produce accurate results. But the dataset size used for this experiment is very small.Al-Ansari et al. [16] suggested an integrated CAD system to screen mammograms that use DL approaches for breast mass detection, segmentation, and classification. You-Only-Look-Once (YOLO) for mass detection. Around 410 mammograms from the INbreast database served as this system's training and testing data. The dataset was small; data augmentation was done on the existing dataset. The images were rotated at 45-degree angles, making 896 mammograms available. Later, transfer learning was used to initialize all the DL model parameters for the segmentation portion. Finally, a simplified version of the AlexNet was utilized to classify the masses as benign or cancerous. The overall success rate of the prediction was 95.64 %. Pawar et al. [9] developed an AI-based MBD classifier using a multichannel DenseNet architecture for breast cancer detection using multichannel Densenet architecture. The architecture comprises a four-channel DenseNet model using transfer learning for extracting the significant features from four views of digital mammograms (two mediolateral oblique (MLO) views and two craniocaudal (CC) views) from a single patient. The performance was assessed using precision, responsiveness, specificity, and the area under the curve (AUC) achieved an accuracy of 96.67% during training and 90.06% during testing, with an average AUC of 0.9625. In another approach for cancer detection. Al-Antari et al. [18] enhanced the effectiveness of deep learning in diagnosing breast lesions. The system comprises three customized deep learning classifiers (ResNet-50, InceptionResNet-V2, and ordinary feedforward CNN) for breast lesion classification and a YOLO detector for breast lesion detection. The classifiers are assessed using 5-fold cross-validation tests on DDSM and INbreast. Mohapatra et al. [19] compared the effectiveness of different CNN architectures, including AlexNet, VGG16, and ResNet50.The models were trained from scratch or fine-tuned using transfer learning with pre-trained weights. When trained from scratch, AlexNet achieved an accuracy of 65%, outperforming other models. Rybiałek et al. [25] explored the potential of DenseNet architectures in classifying breast tissue irregularities, comparing three different DenseNet variants using mammography data. They considered a limited dataset consisting of 2,247 images per class. Training was done using stratified 10-fold cross-validation to achieve statistically reliable estimates of the model's performance metrics. DenseNet-201 was observed to be the best model, giving 0.96 (AUC), 0.92 for precision, 0.90 for recall, and 91% for accuracy. The researchers don't consider the Multiview approach. In contrast, we have considered two mediolateral oblique (MLO) and two craniocaudal (CC) views of each patient to extract the distinct features for breast cancer detection. Mousa et al.[26] integrated a self-attention model into pre-trained DenseNet architectures. The proposed system attained an accuracy of 0.9939, exhibiting the effectiveness of

combining DenseNet with a self-attention model. Despite the approaches mentioned above, breast cancer detection is subjective and done by expert radiologists as objective methods provide mixed results. Deep learning algorithms do not produce more precise results because these are fundamental bottlenecks [17]. Another primary reason behind this is that deep learning algorithms require an enormous data value and authorized ground truth; hence, acquiring a large dataset is another challenge for researchers [18]. In addition to this, mammographic images are vendor-dependent; therefore, all vendor-specific pictures need to make the model more robust. The primary motivation behind this research is to investigate the transfer learning application of different DenseNet architectures to enhance breast cancer classification accuracy.

Notably, various architectures have been designed and developed to examine the significant contribution of four mammography views of a single patient.

Input Dataset

The proposed research uses the publicly available dataset known as a database for screening mammography (DDSM) [19], with demonstrated pathogeny data marked as benign, normal, and malignant. Different data augmentation techniques like random rotating, vertical and horizontal flipping, cropping and zooming are used to enhance the original dataset. A total of 9695 mammograms are used for training and testing purposes. The aspired algorithm utilizes 2421 Right-MLO, 2421 Left_MLO, 1678 R_CC, and 3161 L_CC views. There are a total of 9695 mammographic images, and the distribution for Benign, Cancer and Normal is 3361, 3606 and 2728, respectively. The ground truth of each class is labelled with the help of a specialist radiologist's team into three categories benign, normal, and malignant. Table 1 presents the details of the ground truth input dataset used in this proposed study.

Table-1. Input dataset used for training and validation of the proposed algorithm

Breast cancer class	Total number of Images
Benign	3361
Cancer	3606
Normal	2728
Total	9695

4.0 Proposed Methodology

This segment describes the proposed breast cancer detection technique and is split into three subsections as organized subsequently.

4.1 Preprocessing of digital mammograms

Digital mammography delivers all the edges of digital image processing to improve image quality, which can be additionally valuable for precise breast cancer diagnosis.

Segmentation of Pectoral Muscle

Different researchers have recorded techniques for breast border detection and removal of the artefacts and noise if any. For breast border detection, breast skin-air interface segmentation is a tough job because the intensity of the border of the breast is identical to the background. The above-mentioned reason is the fundamental cause which converts pixels near the border into the background. The unprocessed image contains artifacts, tags and pectoral muscle. In our implementation, artifacts and tags are removed using filters and for pectoral muscle which appears equal white as that of the cancer tissue in mammograms, Breadth First Search (BFS) algorithm is implemented in our prior study. The BFS algorithm starts by identifying the connected components in the image. Starting from a seed point in the right corner, algorithm investigates neighboring pixels to locate the boundaries of the pectoral muscle. Once the pectoral muscle area is

distinguished, the algorithm suppresses this region. This preprocessing step plays a key role in improving the overall performance of the model.

Contrast enhancement

Contrast enhancement is one of the solutions to reduce the noise and enhance the visibility of the image. [22-24] Various image processing methods are suggested by researchers, like Histogram equalization, Wavelet transform (W.T.), Adaptive contrast enhancement (ACE), and Adaptive histogram equalization (AHE). All the above-mentioned methods are demerits in words of noise reduction and processing time [18-21].

The proposed research uses contrast enhancement with AGCWD (Adaptive Gamma Correction with Weighting Distribution) offered by [24]. Eq-1 describes gamma correction and histogram equalization.

$$T(l) = l_{max}(\frac{l}{l_{max}})\gamma \quad (1)$$

Where $lmax$ is max. Intensity of input image and γ is an adaptive parameter. Intensity value lOf image becomes T (l) after gamma correction. This approach's main advantage is that, because of its nonlinear function, extraordinarily dark and light locations are unaffected by mid-tones. This allows for more precise identification of breast border pixel intensity, which helps to widen the breast border. This method also lowers noise at the breast skin-air interface and background, enhancing visibility at the breast border, which helps to create a delicate breast border. The contrast-enhanced version of the input image is illustrated Results of contrast enhancement is shown in Figure-3

(a) (b)

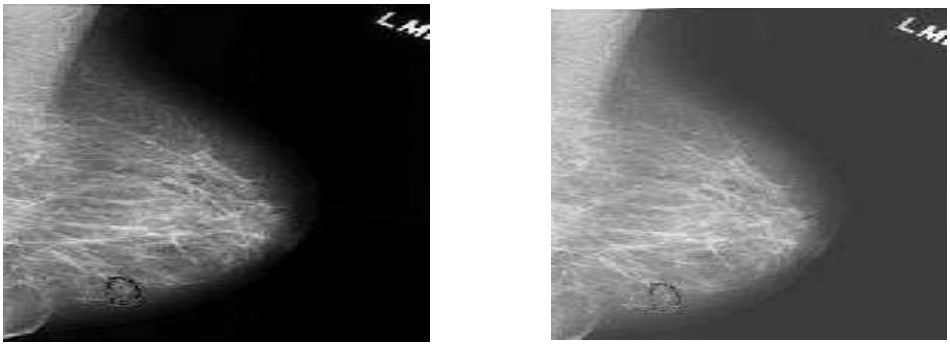

Fig.3- Image enhancement (a) Input image (unclear breast skinair interface) (b) Enhanced image. (Enhancement in the visibility of skin air interface)

The Output Image obtained from the previous stage Fig.3 (b) was used for breast border detection. To identify the breast tissue as a single connected component, local thresholding was performed with four-class multi-otsu thresholding. The primary reason behind the use of multi-otsu thresholding is to find the initial seed for the breadth-first search algorithm. Multi-otsu thresholding optimizes the variance between the classes. Each class acts as a distinct class concerning the intensity values of their pixels. Proposed method uses four classes (C1, C2, C3, and C4) for multi-otsu thresholding. The concept of between-class variance is given by Eq-2.

$$\sigma_b^2 = \sum_{k=1}^{K} P_k(M_k - M_g)^2 \quad (2)$$

where,

International Journal of Environmental Sciences
ISSN: 2229-7359
Vol. 11 No. 9s, 2025
https://theaspd.com/index.php

$$P_k = \sum_{i \in C_k} p_i \quad (3)$$

and

$$M_k = \sum_{i \in C_k} i\, p_i \quad (4)$$

The results of multi-otsu thresholding are illustrated in Fig.4 (b). To select the initial seed, specific observations are performed with different multi-Otsu thresholding image samples. After detailed observations, the image pixel point (150, 20) is identified as an initial seed that will always remain inside the breast and pectoral muscle. In proposed algorithm, after initial seed selection, a breadth -first search is performed from the initial seed point till the threshold value is non-zero. This procedure provides a single connected component as a breast part illustrated in Fig.4(c). After breast part identification, all the tags and artifacts are removed from the background to improve image quality, as shown in Fig.4 (d).

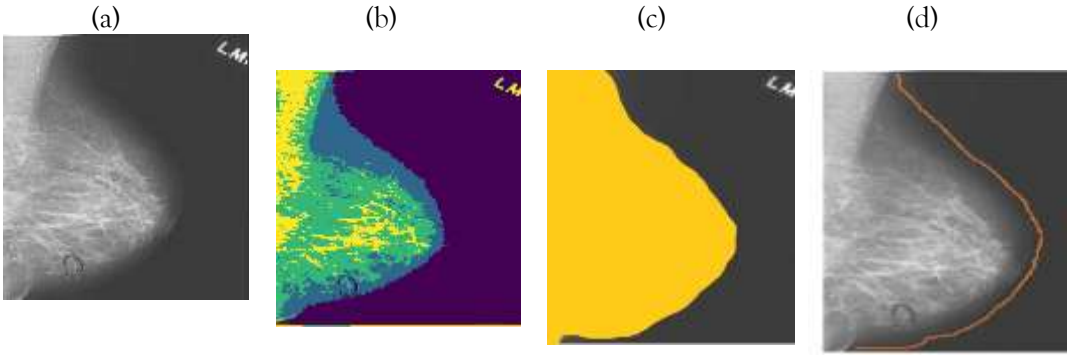

Fig.4- Breast border detection (a) Input mammogram (b) Multiotsu thresholding (four class) (c) Breast as a single connected component (d) Breast border detection and artifacts removal

4.2 Design and development of Dense-Net architecture

This research presents the feature learning capability of Dense-Net architecture's three variants known as DenseNet121, 169, and 201 offered by Huang et al. [10] toward breast cancer detection. The suggested technique utilizes four independent views and a combination of all the views of digital mammography as an input image. Fig 5-7 depicts the details about all three variants of Dense-Net architecture used in this study.

4.2.1 Input convolutional layer

The Input Convolutional Layer is the first layer common to all Dense Net architecture variants. This layer receives the images that need to be processed by the Dense Net model. This layer consists of the convolutional layer and the pooling layer. The convolutional layer consists of 7 x 7 kernels with a stride equal to 2. The essential function of this layer is to generate the feature maps from the input image with the support of the filters or feature detectors. The input convolutional layer is responsible for reducing the size of the input image to dimensions of 112 x 112 x 3. The resizing of the input image causes significant changes in the feature map to overcome this; the resized input image then passes through the second type of layer in the Input Convolutional Layer, which is the pooling layer of 3 × 3 maximum pooling, also with a stride equaling 2. As the name suggests, this pooling layer pools together all the data and calculates the total value in each patch of the feature map. The purpose of this layer is to ensure that small changes in the position do not lead to significant changes in the final output. Thus, the input layer's convolution and pooling operation reduce the input image size to 56 × 56 ×3 before being passed on to the dense blocks.

International Journal of Environmental Sciences
ISSN: 2229-7359
Vol. 11 No. 9s, 2025
https://theaspd.com/index.php

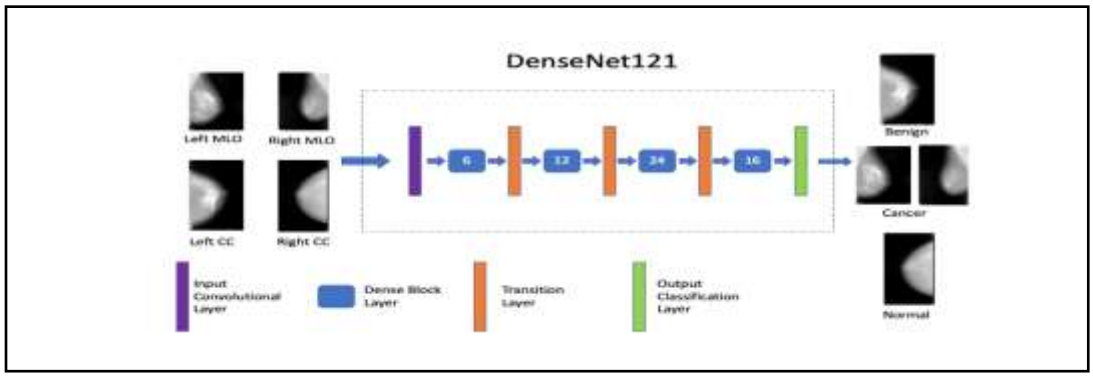

Fig.5- Functional block diagram of DenseNet 121

4.2.2 Dense Block Layer

The next type of layer that comes after the input Layer is the Dense Block Layer. In this dense block, all the features from the layers are extracted using K convolution kernels. The feed-forward connection mechanism is one of the merits of the dense Net, which enhances accuracy and reduces computation. The network growth rate, or parameter k, is referred to as a hyperparameter in Dense Net. The further dense-Net block consists of the bottleneck layer (1 × 1 convolution layer between batch normalization, ReLU, and 3 × 3 convolution layer). The number of times this bottleneck layer repeats in each Dense Block varies from block to block within the same Dense Block and different variants of the Dense Block. This entire dense block layer repeats four times in the whole architecture. After convolution in four dense blocks, each layer is in charge of creating a k-characteristic map, which also keeps the feature maps of each layer uniform in size.

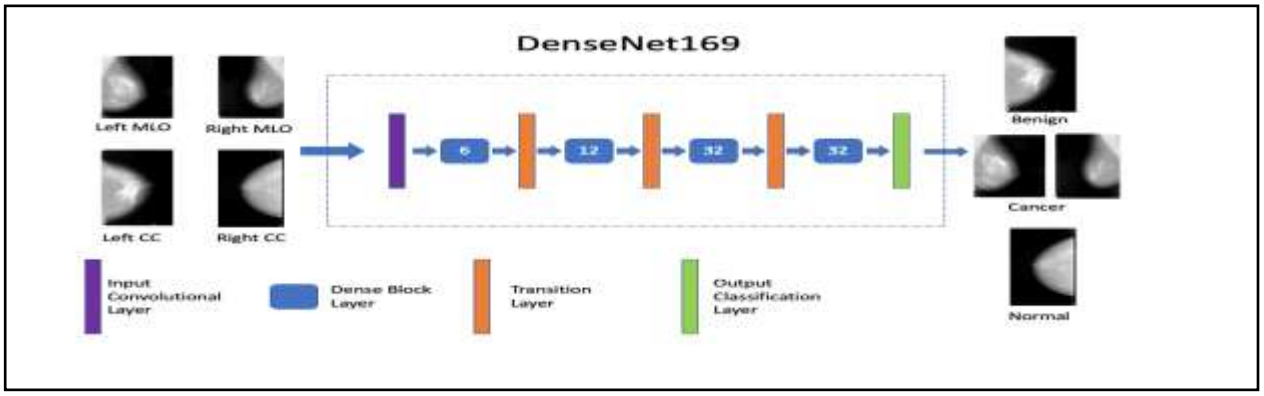

Fig. 6-Functional block diagram of the DenseNet 169

4.2.3 Transition Layer

The transition layer is responsible for making the feature map smaller by merging two nearby dense block layers. The transition layer consists of three layers, a batch normalization layer, and then a 1 × 1 convolution layer, followed by a 2 × 2 average pooling layer. After passing through all these layers within the transition layer, the image size changes to 7 × 7 × 3. The combination of a dense block layer followed by a transition layer is repeated three times and is followed by one last Dense Block Layer. The output of these 8 layers (1

Input Convolutional Layer + 4 Dense Block layers + 3 Transition Layers 1 output layer), Each layer serves as an input for the preceding level, as shown by the following formula Eq-5.

$$X_l = H_l([x_0, x_1 \ldots . x_{l-1}]) \quad (5)$$

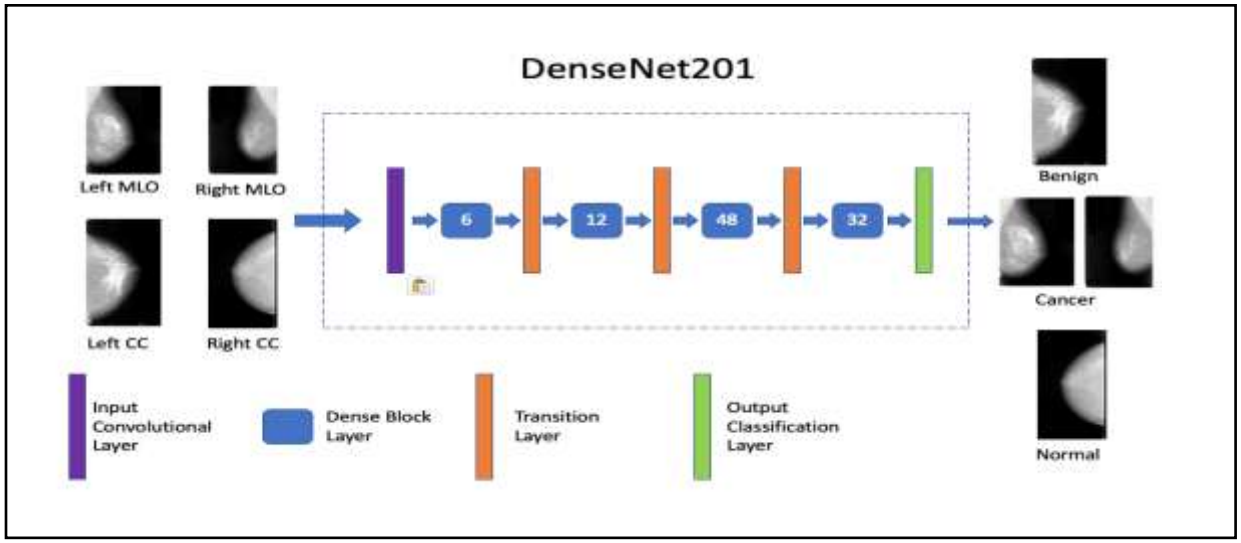

Fig. 7- Functional block diagram of the DenseNet 201

4.2.4 Output Classification Layer

The last and final layer of any Dense Net architecture is the output classification layer. The suggested design's output layer has a global pooling layer to retrieve meaningful information from each channel. The Flatten layer flattens extracted characteristics before transferring them to the individual dense layer. The suggested technique sorts of output into the appropriate class using the SoftMax classifier.

5.0 Experimental analysis and result analysis

The training and testing of the proposed models are performed on the TensorFlow framework on Google Co-laboratory, a free online cloud-based Jupyter notebook environment. All available dataset is divided into training and testing dataset. All the proposed models are trained with the Adaptive Moment Estimation (Adam) algorithm using batch sizes 4 and 150 epochs on the 80% dataset. Adam is an optimization algorithm that combines the 'gradient descent with momentum' algorithm and the Root Mean Square Propagation (RMSP) algorithm. Eq-6-7 defines the gradient descent with momentum in the Adam algorithm.

$$w_{t+1} = w_t - \alpha m_t \quad (6)$$

where,
w_t = weights at time t
α = learning rate
m_t = aggregate of gradients at time t
Eq-7 defines how the aggregate of gradients is calculated (m_t),

$$m_t = \beta m_{t-1} + (1-\beta)\frac{\delta L}{\delta w_t} \quad (7)$$

where,
δL = derivative of Loss Function
δw_t = derivative of weights at time t
β = Moving average parameter
The momentum algorithm accelerates the gradient descent process by employing the "exponentially weighted average" of the gradients. This method converges more quickly to the minima when averages are used. The second technique, RMSP, employs the "exponential moving average" to further optimise the procedure. Eq-8 defines the RMSP used in the Adam algorithm.

$$w_{t+1} = w_t - \left(\frac{\alpha_t}{\sqrt{(v_t+\varepsilon)}} * \frac{\delta L}{\delta w_t}\right) \quad (8)$$

where.
w_t = weights at time t
v_t = sum of square of past gradients
α_t= learning rate at time t
δL = derivative of Loss Function
δw_t = derivative of weights at time t
ε = A small positive constant

Eq-9 defines how the sum of square of past gradients is calculated (v_t),

$$v_t = \beta v_{t-1} + (1-\beta) * \left(\frac{\delta L}{\delta w_t}\right)^2 \quad (9)$$

Where,
β = Moving average parameter
The gradient descent is modified after each iteration to keep it consistent and impartial throughout the procedure. Hence, to provide a more optimised gradient descent, Adam Optimizer relies on the advantages or strong points of the previous two approaches.
The weight correcting step size is the learning rate of the model. The learning rate is a configurable hyperparameter that regulates the rate by which the model learns. The initial learning rate for this model is 0.1 (default value) and split by ten at 50% and or 75% of the total training epochs.
The categorical cross-entropy serves as a loss function in this model, quantifying the distinction between four likelihood distributions. This loss function performs agreeably with the SoftMax activation function in the multiclass category. Eq-10 describes the categorical cross-entropy mathematically, which is:

$$C.E. = -\sum t_i \log(s_i) \quad (10)$$

Where C.E. is cross-entropy t_i and s_i ground truth and the convolutional neural network (CNN) score for each class 'i' in c. Table 2 presents the setting of different hyperparameters used to obtain the optimized results of the proposed architectures.
Table-2 List of the different hyperparameter settings of DenseNet variants

Hyperparameter	**DenseNet121**	**DenseNet121**	**DenseNet121**
Model Initial Learning Rate	0.1	0.1	0.1

Image Size	320 x 320 x 3	320 x 320 x 3	320 x 320 x 3
Batch Size	4	4	4
Target Labels	Ground Truth	Ground Truth	Ground Truth
Data Augmentation	Flipping	Flipping	Flipping
Loss Function	Categorical Cross Entropy	Categorical Cross Entropy	Categorical Cross Entropy
Optimization Algorithm	Adam Optimizer	Adam Optimizer	Adam Optimizer
Validation Parameter	Classification Accuracy	Classification Accuracy	Classification Accuracy

The principal motivation behind this research article is to check the ability of different DenseNet architectures to detect breast cancer with the application of the independent and combinational views of digital mammography. All the available opinions on digital mammography are divided into seven cases: 1. Only Left MLO 2. Only Right MLO 3. Both MLO together 4. Only Left CC 5. Only Right CC 6. Both the CC together and 7. All the views together. This section describes the experimental result analysis of all three variants of the DenseNet architecture. All the models are experimentally tested for 125 epochs with the application of all seven cases of input digital mammograms.

5.1 Experimental test case 1

When all the input cases were applied across Dense-Net 121 Architecture with the same hyperparameter setting mentioned in the previous section, the proposed model provided the following results during testing and training, presented in Table- 3 in which testing and training classification accuracy is given in %.

Table-3 the classification accuracy of DenseNet-121 during training and testing

Sr.No.	**Sample case description**	**% Classification Accuracy**	
		During Training	**During Testing**
1	Only Left MLO	92.32	90.928
2	Only Right MLO	93.10	90.206
3	Both MLO together	90.44	90.923
4	**Only Left CC**	**93.10**	**94.085**
5	Only Right CC	95.11	93.601
6	Both the CC together	92.20	93.763
7	**All the views together**	**88.83**	**90.485**

Confusion matrix of only left CC and the all the views together result cases are depicted in Fig-8

(a)

(b)

International Journal of Environmental Sciences
ISSN: 2229-7359
Vol. 11 No. 9s, 2025
https://theaspd.com/index.php

Fig.8- (a) Confusion matrix for Left CC (b) Confusion matrix for all views together

5.2 Experimental test case 2

Similarly, when all the input cases were applied across Dense-Net 169 model provided classification accuracy during training and testing are shown in Table-4.

Table-4 the classification accuracy of DenseNet-121 during training and testing

Sr.No.	**Sample case description**	**% Classification Accuracy**	
		During Training	**During Testing**
1	Only Left MLO	92.56	91.134
2	Only Right MLO	93.36	90.309
3	Both MLO together	91.61	90.665
4	**Only Left CC**	**94.09**	**94.637**
5	Only Right CC	96.48	93.452
6	Both the CC together	93.09	94.485
7	**All the views together**	**89.78**	**90.975**

Confusion matrix of only left CC and the all the views together result cases are depicted in Fig-9

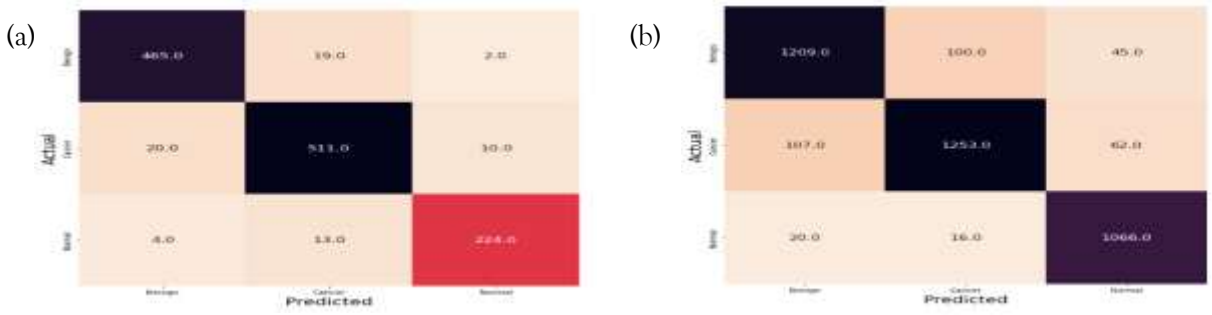

Fig.9- (a) Confusion matrix for Left CC (b) Confusion matrix for all views together

5.3 Experimental test case 3

Similarly, when all the input cases were applied across Dense-Net 201 model provided classification accuracy during training and testing are shown in Table-5.

Table-5 the classification accuracy of DenseNet-201 during training and testing

Sr.No.	**Sample case description**	**% Classification Accuracy**	
		During Training	**During Testing**
1	Only Left MLO	93.33	91.753
2	Only Right MLO	93.49	90.412
3	Both MLO together	92.20	91.336
4	**Only Left CC**	**94.90**	**96.924**
5	Only Right CC	96.72	94.048
6	Both the CC together	94.02	95.00
7	**All the views together**	**91.11**	**90.975**

International Journal of Environmental Sciences
ISSN: 2229-7359
Vol. 11 No. 9s, 2025
https://theaspd.com/index.php

Confusion matrix of only left CC and the all the views together result cases are depicted in Fig-10

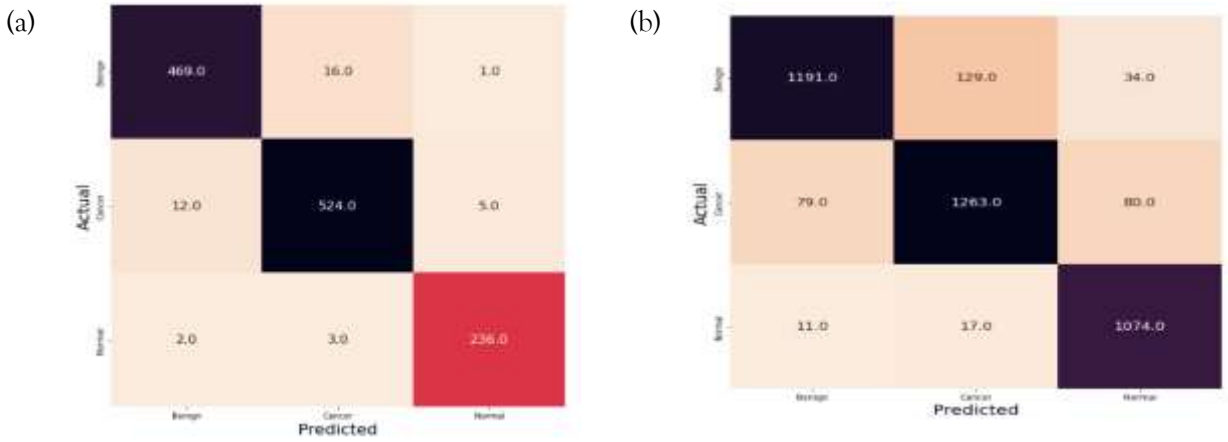

Fig.10- (a) Confusion matrix for Left CC (b) Confusion matrix for all views together

5.4 Result analysis

The proposed variant of DenseNet architecture was analyzed using the confusion matrix on the test dataset. Figure 8,9,10 depicts the heat maps of the proposed architecture, which further helps to analyze which category was accurately classified. A darker diagonal indicates the correct classification rate. The proposed models organize all the classes but found a little bit confused between benign and cancer. Further evaluations of the classification results are performed with precision, recall and F1-score. Among those parameters, precision is the ration of proportion of samples with optimistic forecasts affecting the total numeral of accurate praising samples. The recall ratio of precisely anticipated samples to the entire samples and the F1-score is the ratio of precision and recall weight.

Eq. [11-13] define the precision, recall, and the F1-score.

$$\text{Precision} = \frac{TP}{TP+FP} \tag{11}$$

$$\text{Sensitivity/Recall} = \frac{TP}{TP+FN} \tag{(12)}$$

$$\text{F1-Score} = \frac{2}{\frac{1}{\text{Precision}}+\frac{1}{\text{Recall}}} = \frac{2*(\text{Precision}*\text{Recall})}{\text{Precision}+\text{Recall}} \tag{13}$$

Where, TP = True Positive
FP = False Positive
FN = False Negative

Table 6-8 highlights all the model's performance of all the possible samples

International Journal of Environmental Sciences
ISSN: 2229-7359
Vol. 11 No. 9s, 2025
https://theaspd.com/index.php

Table-6 Presents the performance parameters of the DenseNet 121 Architecture

DenseNet121	Case 1			Case 2			Case 3			**Case 4**		
Case	B	C	N	B	C	N	B	C	N	**B**	**C**	**N**
Precision	0.864	0.959	0.900	0.905	0.915	0.882	0.898	0.934	0.895	**0.950**	**0.953**	**0.900**
Recall	0.938	0.840	0.986	0.873	0.880	0.969	0.911	0.850	0.985	**0.942**	**0.928**	**0.951**
F1 Score	0.900	0.896	0.941	0.889	0.898	0.924	0.905	0.890	0.938	**0.946**	**0.940**	**0.925**
DenseNet121	Case 5			Case 6			**Case 7**					
Case	B	C	N	B	C	N	**B**	**C**	**N**			
Precision	0.892	0.959	0.946	0.939	0.915	0.966	**0.913**	**0.906**	**0.895**			
Recall	0.925	0.857	1.000	0.910	0.933	0.975	**0.881**	**0.878**	**0.964**			
F1 Score	0.908	0.905	0.972	0.924	0.924	0.970	**0.897**	**0.892**	**0.928**			

B- Benign, C- Cancer and N- Normal

In the above table, the highlighted version indicates that the model can perform better classification when only the left CC view is there compared to all the mammography views. Figure 11 depicts the accuracy and validation loss of DenseNet 121 architecture during training and validation.

(a)

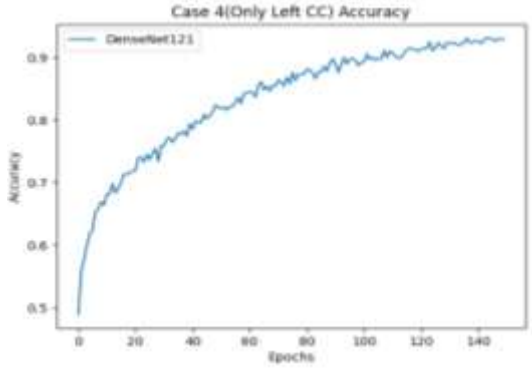

(b)

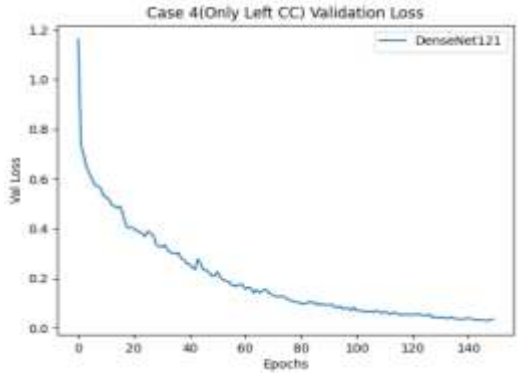

(c)

(d)

International Journal of Environmental Sciences
ISSN: 2229-7359
Vol. 11 No. 9s, 2025
https://theaspd.com/index.php

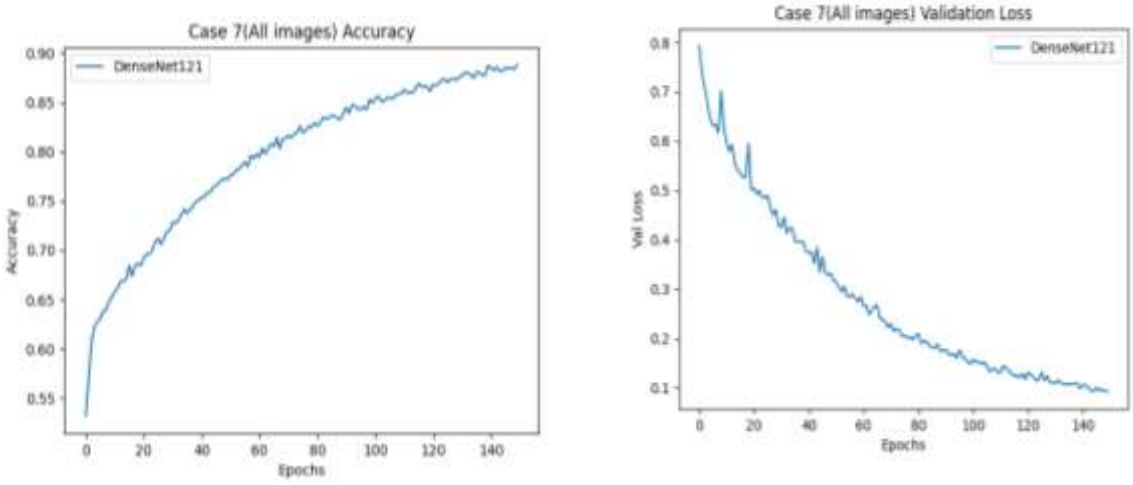

Fig.11 (a) Classification accuracy and (b) validation loss for only left views (c) classification accuracy and (d) validation loss for All the views together.

Table-7 Presents the performance parameters of the DenseNet 169 Architecture

DenseNet169	Case 1			Case 2			Case 3			**Case 4**		
Case	B	C	N	B	C	N	B	C	N	**B**	**C**	**N**
Precision	0.876	0.947	0.905	0.883	0.934	0.887	0.866	0.908	0.959	**0.951**	**0.941**	**0.949**
Recall	0.921	0.863	0.979	0.914	0.860	0.947	0.904	0.873	0.966	**0.957**	**0.945**	**0.896**
F1 Score	0.898	0.903	0.940	0.899	0.895	0.916	0.884	0.890	0.963	**0.954**	**0.943**	**0.922**
DenseNet169	Case 5			Case 6			**Case 7**					
Case	B	C	N	B	C	N	**B**	**C**	**N**			
Precision	0.908	0.954	0.937	0.927	0.945	0.966	**0.905**	**0.915**	**0.909**			
Recall	0.925	0.853	1.000	0.941	0.924	0.978	**0.893**	**0.881**	**0.971**			
F1 Score	0.916	0.900	0.967	0.934	0.935	0.972	**0.899**	**0.898**	**0.939**			

Figure 12 depicts the accuracy and validation loss of DenseNet 169 architecture during training and validation.

(a) (b)

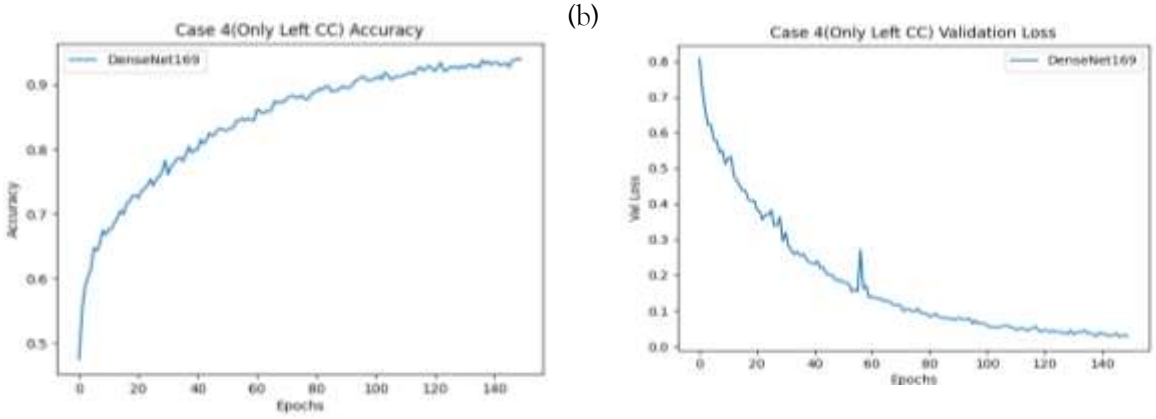

International Journal of Environmental Sciences
ISSN: 2229-7359
Vol. 11 No. 9s, 2025
https://theaspd.com/index.php

(c) (d)

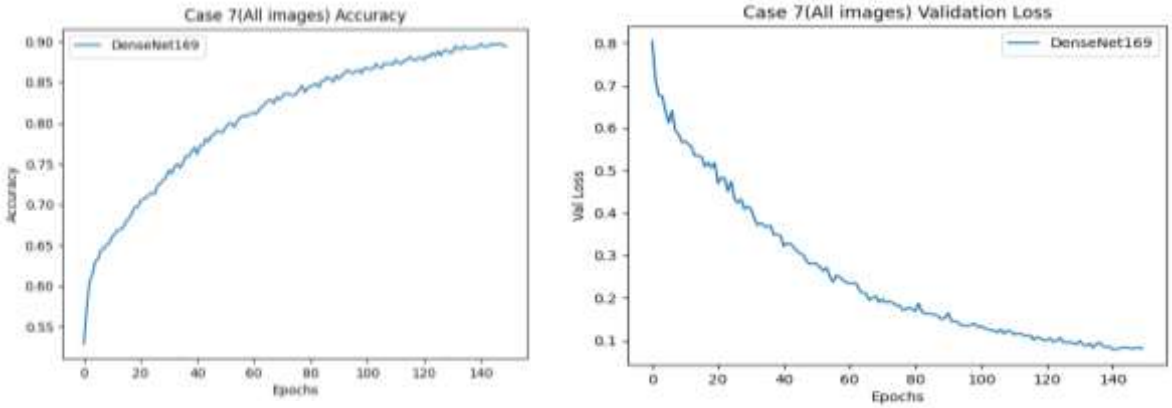

Fig.12 (a) Classification accuracy and (b) validation loss for only left views (c) classification accuracy and (d) validation loss for All the views together

Table-7 Presents the performance parameters of the DenseNet 201 Architecture

DenseNet201	Case 1			Case 2			Case 3			**Case 4**		
Case	B	C	N	B	C	N	B	C	N	**B**	**C**	**N**
Precision	0.867	0.940	0.942	0.889	0.894	0.937	0.906	0.903	0.936	**0.971**	**0.965**	**0.975**
Recall	0.921	0.873	0.986	0.867	0.898	0.962	0.895	0.890	0.967	**0.965**	**0.969**	**0.975**
F1 Score	0.893	0.905	0.964	0.878	0.896	0.949	0.900	0.896	0.951	**0.968**	**0.967**	**0.975**
DenseNet201	Case 5			Case 6			**Case 7**					
Case	B	C	N	B	C	N	**B**	**C**	**N**			
Precision	0.914	0.950	0.949	0.930	0.953	0.973	**0.930**	**0.896**	**0.904**			
Recall	0.925	0.871	1.000	0.955	0.921	0.975	**0.880**	**0.888**	**0.969**			
F1 Score	0.919	0.909	0.974	0.942	0.937	0.974	**0.904**	**0.892**	**0.936**			

Figure 13- depicts the accuracy and validation loss of DenseNet 201 architecture during training and valida

(a) (b)

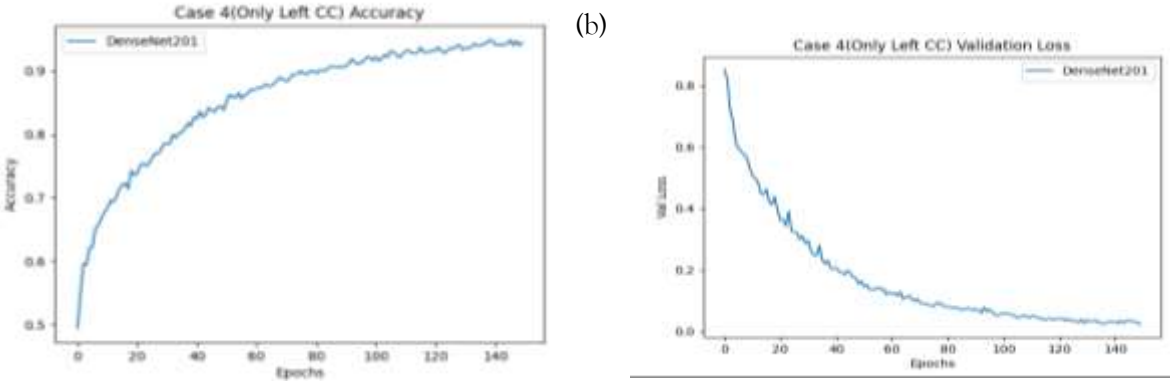

(c) (d)

International Journal of Environmental Sciences
ISSN: 2229-7359
Vol. 11 No. 9s, 2025
https://theaspd.com/index.php

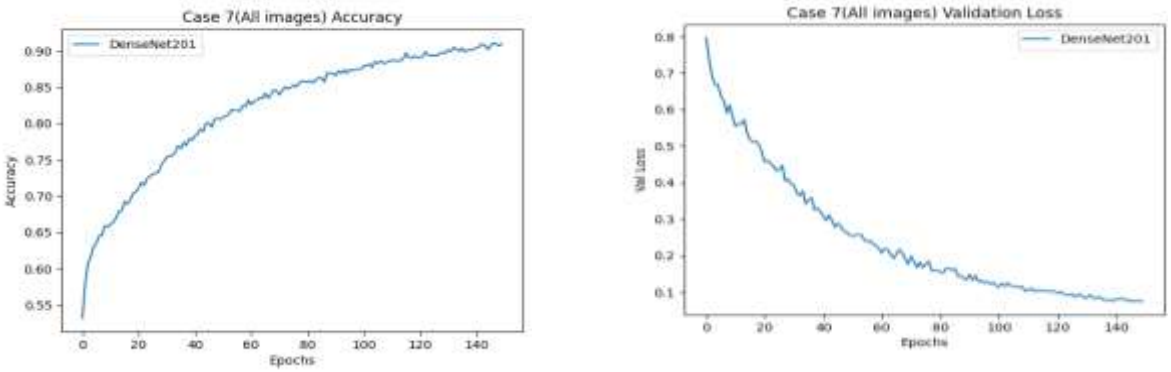

Fig.13 (a) Classification accuracy and (b) validation loss for only left views (c) classification accuracy and (d) validation loss for All the views together

DISCUSSION

Generally, Radiologists support all the views to detect breast cancer. The proposed research investigates an AI-based approach to predicting breast cancer from different mammography views. This method uses the effect of three models in several experimental settings using different mammographic views. In this approach, different end-to-end DenseNet variants are used to extract various features of digital mammography for breast cancer detection. The essential motivation is to check whether the classification accuracy of deep learning models depends on the individual mammographic views. The proposed research utilizes 9695 digital mammography images for this study. All input images are classified into three categories, Benign, Cancer, and Normal, with the help of expert radiologists as ground truth. Three classifiers, DenseNet 121, 169, and 201, are used to check the performance of all the available opinions on digital mammography, which are divided into seven cases: 1. Only Left MLO 2. Only Right MLO 3. Both MLO together 4.Only Left CC 5.Only Right CC 6. Both the CC together and 7. All the views together. The primary finding behind this research article is that all the proposed models provided better classification accuracy on Left CC views and worst performance when all the views are used together.

A short comparison of the proposed models is highlighted in Table-8.

Table 8- Comparative analysis of the all DenseNet models on different views

Sr.No.	**Sample-Case Description**	**% Classification Accuracy**		
		DenseNet-121	DenseNet-169	DenseNet-201
1	Only Left MLO	90.928	91.134	91.753
2	Only Right MLO	90.206	90.309	90.412
3	Both MLO together	90.923	90.665	91.336
4	**Only Left CC**	**94.085**	**94.637**	**96.924**
5	Only Right CC	93.601	93.452	94.048
6	Both the CC together	93.763	94.485	95.00
7	**All the views together**	**90.485**	**90.975**	**90.975**

The proposed model is comparable with other existing state of art modes which is provided in Tabular form in Table-9.

Table 9 -Comparative analysis of proposed method

References	**Dataset**	**Proposed Method**	**Classification Accuracy**

Zheng et al .[15]	UCHCDM – 102	Object Detection + Feature Extraction using CNN + classifying using RNN	0.991
Li et al .[24]	2042	DenseNet-II architecture	94.55%
Mohapatra et al. [25]	Mini-DDSM - 9752	AlexNet, VGG16 and ResNet50	AlexNet and VGG16 - 65%, ResNet50 - 61%
AlEisa et al. [27]	CBIS-DDSM - 2620	Fully Convolutional Neural Networks and Beta Wavelength auto encoder	93%
Al-antari et al .[28]	INbreast – 410	You-Look-Only-Once approach based Full resolution Convolutional Neural Network (FrCN)	95.64%
Kishore Khan 2024	CBIS-DDSM	DenseNet121 with a residual model (RM-DenseNet)	96.50%
Samudrala et al. [32]	Histological dataset	DenseNet-121 model + Attention based pyramid scene parsing network (Att-PSPnet).	94.68%
Rybiałek et al. [25]	2247	DenseNet 121,169,201	91%
Proposed method	**DDSM -9695**	**Dense-Net variants**	**96.92%**

From comparative analysis following are the results outcome of this study, when model inputs are Left CC then each model has provided higher accuracy. Among all, Dense-Net 201 has provided 96.92% accuracy. In Multiview analysis all the models are recorded with less classification accuracy. The lowest classification accuracy is recorded at 90. Samudrala et al. [32]. performed the hybrid semantic segmentation networks that were introduced. Initially, the input image sets are applied to the pre-processing phase and, after that, subject to the segmentation process. Adaptive Local Gamma Correction (ALGC) enhanced the image contrast. The semantic segmentation topology was done by using the hybrid network of the DenseNet-121 model with an attention-based pyramid scene parsing network (Att-PSPnet). The Att-PSPnet network handled the extraction of the feature map and scene parsing. The Attention Gate mechanism improved the quality of the high-dimensional hidden layer features. The pyramid dilated convolution module (PDM) is used to enhance accuracy and to make efficient decisions. The proposed method achieves 94.68% prediction accuracy, higher than the existing approaches.Out of all DenseNet 201 provided a superior view to the other two variants. From these results, we can conclude that deep learning classifiers provide less classification when we provide the mixed views.

CONCLUSION

In summary, the fundamental objective of this study is to classify breast cancer automatically. The study presents the novel method of Multiview analysis of mammographic images with DenseNet121, 169, and 201 architectures. The proposed structure utilises the four views of a single patient to improve feature learning power through a Multiview approach. In the method, image contrast enhancement and pre-processing of the input image are implemented to enhance the condition of the training image data. The input images are

processed through different Dense-Net architectures to extract and fuse all the features. Analysis of the results suggests that the proposed model efficiently distinguishes between all classes but predominantly provides strong results on left CC views compared to other views. The best classification accuracy of the proposed model is recorded at 96.92 by Dense-Net 201 compared to other models. The introduced design consists of some weaknesses that have been discussed and will be addressed in the prospective study; with modifications, the proposed method is appropriate for application in clinical workflow in breast cancer screening to avoid false recalls.

REFERENCES

1. Advani, P., & Moreno-Aspitia, A. (2014). Current strategies for the prevention of breast cancer. Breast Cancer: Targets and Therapy, 59-71.https://www.tandfonline.com/doi/abs/10.2147/BCTT.S39114
2. Kamangar, F., Dores, G. M., & Anderson, W. F. (2006). Patterns of cancer incidence, mortality, and prevalence across five continents: defining priorities to reduce cancer disparities in different geographic regions of the world. Journal of clinical oncology, 24(14), 2137-2150.https://ascopubs.org/doi/abs/10.1200/JCO.2005.05.2308
3. Sapate, S., Talbar, S., Mahajan, A., Sable, N., Desai, S., & Thakur, M. (2020). Breast cancer diagnosis using abnormalities on ipsilateral views of digital mammograms. Biocybernetics and Biomedical Engineering, 40(1), 290-305.https://www.sciencedirect.com/science/article/pii/S0208521618304996
4. Gadekallu, T. R., Iwendi, C., Wei, C., & Xin, Q. (2021). Identification of malnutrition and prediction of BMI from facial images using real-time image processing and machine learning. IET Image Process, 16, 647-658..
https://pdfs.semanticscholar.org/1f59/e54001177de23c9306c4e194996825adc7be.pdf
5. Sapate, S. G., Mahajan, A., Talbar, S. N., Sable, N., Desai, S., & Thakur, M. (2018). Radiomics based detection and characterization of suspicious lesions on full field digital mammograms. Computer methods and programs in biomedicine, 163, 1-20.https://www.sciecedirect.com/science/article/pii/S0169260717306223
6. Joshi, P. T., Saini, G. S., & Pawar, S. D. (2023, December). Comparative Analysis of Different Preprocessing Techniques for Digital Mammograms Towards Breast Cancer Detection. In 2023 6th International Conference on Advances in Science and Technology (ICAST) (pp. 234-239). IEEE.. https://ieeexplore.ieee.org/abstract/document/10454964/
7. Pawar, S., Joshi, P., Sharma, K., & Sapate, S. (2023, June). Review on pre-processing algorithms for breast density classification using digital mammograms. In AIP Conference Proceedings (Vol. 2717, No. 1). AIP Publishing.
8. Lee, J., & Nishikawa, R. M. (2018). Automated mammographic breast density estimation using a fully convolutional network. Medical physics, 45(3), 1178-1190.https://aapm.onlinelibrary.wiley.com/doi/abs/10.1002/mp.12763
9. Pawar, S. D., Sharma, K. K., Sapate, S. G., Yadav, G. Y., Alroobaea, R., Alzahrani, S. M., & Hedabou, M. (2022). Multichannel DenseNet architecture for classification of mammographic breast density for breast cancer detection. Frontiers in Public Health, 10, 885212.https://www.frontiersin.org/articles/10.3389/fpubh.2022.885212/full
10. Huang, G., Liu, Z., Van Der Maaten, L., & Weinberger, K. Q. (2017). Densely connected convolutional networks. In Proceedings of the IEEE conference on computer vision and patternrecognition (pp.4700-4708).
http://openaccess.thecvf.com/content_cvpr_2017/html/Huang_Densely_Connected_Convolutional_CVPR_2017_paper.html
11. Eroğlu, Y., Yildirim, M., & Çinar, A. (2021). Convolutional Neural Networks based classification of breast ultrasonography images by hybrid method with respect to benign, malignant, and normal using mRMR. Computers in biology and medicine, 133, 104407.https://www.sciencedirect.com/science/article/pii/S0010482521002018
12. Shen, L. (2017). End-to-end training for whole image breast cancer diagnosis using an all convolutional design. arXiv preprint arXiv:1711.05775.
https://arxiv.org/abs/1711.05775
13. Ragab, D. A., Sharkas, M., Marshall, S., & Ren, J. (2019). Breast cancer detection using deep convolutional neural networks and support vector machines. PeerJ, 7, e6201.https://peerj.com/articles/6201/
14. Dhungel, N., Carneiro, G., & Bradley, A. P. (2017). A deep learning approach for the analysis of masses in mammograms with minimal user intervention. Medical image analysis, 37,114-128.
https://www.sciencedirect.com/science/article/pii/S136184151730018X
15. Zheng, Yufeng & Yang, Clifford & Wang, Hongyu. (2020). Enhancing breast cancer detection with recurrent neural network. Zheng, Yufeng & Yang, Clifford & Wang, Hongyu. (2020). Enhancing breast cancer detection with recurrent neural network. https://www.spiedigitallibrary.org/conference-proceedings-of-spie/11399/113990C/Enhancing-breast-cancer-detection-with-recurrent-neural-network/10.1117/12.2558817.short
16. Al-antari, Mugahed A. & Al-masni, Mohammed & Choi, Mun-Taek & Han, Seung-Moo & Kim, Tae-Seong. (2018). A fully integrated computer-aided diagnosis system for digital X-ray mammograms via deep learning detection, segmentation, and

classification. International Journal of Medical Informatics. https://www.sciencedirect.com/science/article/pii/S1386505618302880
17. Pawar S, Sapate S, Sharma K. Machine learning approach towards mammographic breast density measurement for breast cancer risk prediction: an overview. Proc ICAST. (2020) 2020:1–14. https://papers.ssrn.com/sol3/papers.cfm?abstract_id=3599187
18. Shivaji D. Pawar, Kamal Kr. Sharma, Suhas G. Sapate, Geetanjali Y. Yadav, Segmentation of pectoral muscle from digital mammograms with depth-first search algorithm towards breast density classification, Bio cybernetics and Biomedical Engineering, Volume 41, i ssue 3,2021,Pages 1224-1241,ISSN 0208-5216,
https://doi.org/10.1016/j.bbe.2021.08.005.
19. Heath M, Bowyer K, Kopans D, Moore R, Kegelmeyer WP. International workshop on digital mammography. Toronto, ON: Med Physics in Proceedings of IWDM (2001). https://www.frontiersin.org/articles/10.3389/fpubh.2022.885212/full
20. M. Zeng, Y. Li, Q. Meng, T. Yang, J. Liu Improving histogram-based image contrast enhancement using gray-level information histogram with application to X-ray images Optik (Stuttg), 123 (2012), pp. 511-520, https://www.sciencedirect.com/science/article/pii/S003040261100249X
21. H. Öktem, K. Egiazarian, J. Niittylahti, J. Lemmetti An approach to adaptive enhancement of diagnostic X-ray images EURASIP J Appl Signal Processing, 2003 (2003), pp. 430-436, https://link.springer.com/article/10.1155/S1110865703211069
22. G. Deng, A generalized unsharp masking algorithm, IEEE Trans Image Process, 20 (2011), pp. 1249-1261, 10.1109/TIP.2010.2092441. https://ieeexplore.ieee.org/abstract/document/730397/
23. D.C. Chang, W.R. Wu, Image contrast enhancement based on a histogram transformation of local standard deviation. IEEE Trans Med Imaging, 17 (1998), pp. 518-531, 10.1109/42.730397. https://ieeexplore.ieee.org/abstract/document/730397/
24. S.C. Huang, F.C. Cheng, Y.S. Chiu Efficient contrast enhancement using adaptive gamma correction with weighting distribution.IEEE Trans Image Process, 22 (2013), pp. 1032-1041, 10.1109/TIP.2012.2226047. https://link.springer.com/chapter/10.1007/978-3-030-47679-3_23
25. Rybiałek, A., & Jeleń, Ł. (2020, May). Application of densenets for classification of breast cancer mammograms. In International Conference on Computer Information Systems and Industrial Management (pp. 266-277). Cham: Springer International Publishing. https://link.springer.com/chapter/10.1007/978-3-030-47679-3_23
26. Mousa, T. E., Zouari, R., & Baklouti, M. (2023, November). Breast Cancer Detection Based DenseNet with Attention Model in Mammogram Images. In International Conference on Model and Data Engineering (pp. 259-271). Cham: Springer Nature Switzerland. https://link.springer.com/chapter/10.1007/978-3-031-49333-1_19
27. Mohapatra, S., Muduly, S., Mohanty, S., & Moharana, S. K. (2022, February). Evaluation of deep learning models for detecting breast cancer using mammograms. In International Conference on Metaheuristics in Software Engineering and its Application (pp. 104-112). Cham:Springer International Publishing. https://www.sciencedirect.com/science/article/pii/S2666412722000162
28. Abed, A. A., & Emadi, M. (2023). Detection and Segmentation of Breast Cancer Using Auto Encoder Deep Neural Networks. Majlesi Journal of Telecommunication Devices, 12(4), 209-217. https://journals.iau.ir/article_709044_a34b7883c1f86a616d8c125decdd3518.pdf
29. Antari. M. A, M. Al-masani and T.-S. Kim, "Deep Learning Computer-Aided Diagnosis for Breast Lesion in Digital Mammogram," Deep Learning in Medical Image Analysis: Challenges and Applications, pp. 59-72, 2020. https://link.springer.com/chapter/10.1007/978-3-030-33128-3_4
30. Khan, S. K., Kanamarlapudi, A., & Singh, A. R. (2024, May). RM-DenseNet: An Enhanced DenseNet Framework with Residual Model for Breast Cancer Classification Using Mammographic Images. In 2024 2nd International Conference on Advancement in Computation & Computer Technologies (InCACCT) (pp. 711-715). IEEE. https://doi.org/10.1109/InCACCT61598.2024.10551125
31. Pawar, S. D., Joshi, P. T., Savalkar, V. A., Sharma, K. K., & Sapate, S. G. (2022, August). Past, present and future of automated mammographic density measurement for breast cancer risk prediction. In Journal of Physics: Conference Series (Vol. 2327, No. 1, p. 012076). IOP Publishing.
32. Samudrala, S., & Mohan, C. K. (2024). Semantic segmentation of breast cancer images using DenseNet with proposed PSPNet. Multimedia Tools and Applications, 83(15), 46037-46063. https://doi.org/10.1007/s11042-023-17411-5